

Article

Numerical Modeling of PD Pulses Formation in a Gaseous Void Located in XLPE Insulation of a Loaded HVDC Cable

Paweł Mikrut *  and Paweł Zydrón * 

Department of Electrical and Power Engineering, AGH University of Krakow, al. Mickiewicza 30, 30-059 Krakow, Poland

* Correspondence: mikrut@agh.edu.pl (P.M.); pzydron@agh.edu.pl (P.Z.)

Abstract: Power cables are one of the key components of fast-growing HVDC transmission systems. The long-term reliability of HVDC cables is closely related to the occurrence of partial discharges (PDs) in their insulation systems. The article analyzes the conditions for the formation of PD pulses in gaseous voids located in the XLPE insulation of an HVDC cable. For this purpose, the MATLAB[®] procedure and the coupled electro-thermal simulation model implemented in COMSOL Multiphysics[®] software were used. The FEM model was used to study the effect of the applied voltage, the temperature field (created in the insulation of the loaded cable) and the location of the gaseous void (on cable radius) in the distribution and values of the electric field in the cable insulation. The model takes into account the influence of temperature and the electric field on the conductivity of the insulating material and relates the value of the PD inception field to the temperature/pressure of the gas inside the void. In the numerical simulation procedure, the time sequences of PDs arising in the gaseous defects of the HVDC cable insulation were analyzed, by observing changes caused by the increase in the temperature of the cable core. The model was used for a study of conditions for PD formation in models of three HVDC cables, for DC voltages from 150 kV to 500 kV. The critical dimensions of gaseous voids were also estimated for each of the analyzed cables, i.e., the dimension which, if exceeded, makes a void a source of PD.

Keywords: HVDC cables; partial discharges (PDs); XLPE; FEM simulation; coupled electro-thermal field



Citation: Mikrut, P.; Zydrón, P. Numerical Modeling of PD Pulses Formation in a Gaseous Void Located in XLPE Insulation of a Loaded HVDC Cable. *Energies* **2023**, *16*, 6374. <https://doi.org/10.3390/en16176374>

Academic Editor: Mario Marchesoni

Received: 21 June 2023

Revised: 30 August 2023

Accepted: 31 August 2023

Published: 2 September 2023



Copyright: © 2023 by the authors. Licensee MDPI, Basel, Switzerland. This article is an open access article distributed under the terms and conditions of the Creative Commons Attribution (CC BY) license (<https://creativecommons.org/licenses/by/4.0/>).

1. Introduction

Alternating current (AC) and direct current (DC) transmission systems are designed and implemented using overhead transmission lines and power cable lines [1–7]. Since the beginning of the power industry, the constantly growing demand of world societies and economies for electricity implies the need to increase the rated voltage of these systems. The choice of the type of system voltage (AC or DC) depends on the transmission distance and/or the location of generation sources and power consumption areas [6–8]. Economic considerations, taking into account investment and operating costs estimated over a long time horizon, play an important role in the decision on the selection of a transmission system [9,10]. In many cases, HVDC (and UHVDC) systems have better technical and economic performance than HVAC (UHVAC) systems. Currently, these systems are used for:

- Long-distance, high-capacity transmission of electric energy [1–3,7];
- The implementation of inter-system connections (usually for non-synchronized systems) [11,12];
- submarine electrical energy transmission [4].

The latter group includes the transmission of electricity from offshore wind farms, especially those located far from the shoreline, in deep water areas. In recent years, the number of such HVDC system implementations has been growing significantly in different regions of the world [10,13–15].

In each of the above-mentioned applications, the very high reliability of the electrical insulation systems is of key importance for the failure-free operation of the entire system. To achieve this goal, HVDC cable production technologies are being improved, based on analyses and model research for estimating the product lifetime, taking into account the factors influencing the rate of insulation aging. The basic stresses causing structural changes in the insulation, the formation and development of defects and the shortening of the effective lifetime of the insulation system include: thermal (T), electrical (E), ambient (A) and mechanical (M) stresses, collectively referred to as TEAM [16,17].

The effective lifetime of the cable insulation is estimated based on aging models that take into account both intrinsic and extrinsic aging processes [4,5,18–24]. In the case of HVDC cable lines, one of the potential causes of reduced reliability is the occurrence of various types of defects in the insulation of cables or cable joints. Some of them are the effects of imperfect technological production processes, whereas others arise as a result of errors made during the laying of the cable line or are the effect of various types of stresses during its operation. The required high quality and reliability of cable insulation can be significantly reduced due to extrinsic aging processes and the related occurrence of various types of defects in the insulation [25,26]:

- Gaseous voids;
- Delaminations;
- Protrusions;
- Contaminations;
- Electrical trees;
- Water trees.

The problems of the occurrences of these types of defects in insulation have been intensively studied, both during non-standard experimental tests and type tests, including long-term tests on model samples, prototypes and complete devices, as well as using various types of numerical simulation tools. Due to the specific nature of the problem resulting from the use of high DC voltage, the methods used for testing AC insulation are not always adequate for use in the analysis and testing of HVDC insulation.

A recognized but still current research problem is the development of electrical and water treeing processes in the polymer insulation of HV cables [27–30]. For example, the problems of the development of electrical trees in HVDC insulation in various operating conditions were analyzed in the research presented in article [31]. The influence of HVDC voltage polarity on the development of electrical trees and partial discharge parameters was also studied [30–33]. Simulation tools using the finite element method implemented in COMSOL software were used to study the conditions and processes of the development of water trees in the XLPE insulation of submarine cables [34,35].

The research described in this paper concerns the determination of the conditions for the formation of partial discharges in the gaseous voids of the XLPE insulation of HVDC cables and the analysis of the time sequences of PD pulses generated as a result of discharge inception. The problem of voids in the insulation of modern XPLE cables concerns the presence of defects in the polymer insulation structure of small size ($\sim 60 \mu\text{m}$) or even smaller, where partial discharges (PDs) may occur [36–38]. The inception of PDs in internal voids in solid insulation is possible when the local electric field inside the void exceeds the value of the PD inception field [39,40]. For AC 50/60 Hz systems, the distribution of the electric field in the cable insulation depends on the permittivity (dielectric constant) of the insulation material [41,42]. In contrast, for DC systems, the distribution of the electric field in the cable insulation is determined by the volume conductivity/resistivity of the insulating material. Due to the dependence of this material parameter on temperature and local electric field values, the E field strength analysis in a DC cable must take into account the influence of these factors on the field distribution in cable insulation for steady and transient states [41–46].

The distribution of the E field strength in the HVDC cable is affected by the space charge accumulated in the insulation (both homocharges and heterocharges trapped in

the bulk of a dielectric), the presence of which may increase or decrease the local field strength [47,48]. For this reason, it is required that new materials intended for extruded cable insulation have very low or even no ability to accumulate space charge [48–51]. For the developed HVDC XLPE 500 kV systems, a certain solution to the problem of space charge accumulation was reported, and confirmed in qualification tests up to 90 °C [52–54]. The test results presented in [54] show that the *field enhancement factor* (FEF), defined by the ratio of the E field strength in the DC-XLPE insulation, taking into account the effect of space charge, to the E field strength without this charge, was always less than 1.10 for 20 kV/mm and 50 kV/mm at 30 °C. In a longer period of time after the application of the DC voltage, it decreased to a value of about 1.05.

For design and operational purposes, extended analyses of temperature and electric field strength distributions in the insulation of HVDC power cables and their accessories are performed. The static and dynamic analyses take into account the geometry of the cable structure, the dielectric material parameters, the processes of space charge accumulation and decay, the effects of reversing the polarity of the DC voltage (in the case of using LCC technology), the presence of PD sources and the influence of DC voltage ripple [6–8,55–58]. One of the basic reasons for the analyses is the estimation of the permissible current-carrying capacity of DC cable lines due to the limit parameters of the insulating material [55,59]. Such analyses are also performed to determine the expected lifetime of the HVDC insulation of cable designed to operate in the planned electro-thermal conditions [60,61].

The article presents an analysis of the influence of the position of the gaseous void in the XLPE insulation of the HVDC cable on the conditions of PD formation and the generation of the PD pulse sequences. In the numerical simulations, made using the finite element method (FEM) in COMSOL Multiphysics® 6.0 software, the presence of an electric field, modified by the influence of the temperature field, in the XLPE insulation of the loaded HVDC cable was taken into account. On this basis, using a dedicated program implemented in MATLAB® R2021b software, conditions for PD formation and time sequences of PD pulses generated at DC voltage were analyzed. Based on the results of numerical simulations, the critical dimension of the gaseous voids was also estimated, depending on its location on the radius of the cable.

2. The Problem of PD Formation and the Numerical Model of the DC Cable

2.1. PD Formation in Gaseous Void—Overview

The formation of streamer PD pulses in a gaseous cavity located in a solid dielectric occurs when two required conditions are met simultaneously [39,40]:

- (1) The electric field strength in the void must exceed the value of the discharge inception field strength;
- (2) As a result of volume or surface processes, an initial electron must be present to trigger the development of the discharge process.

The PD inception field strength E_{inc} inside the gaseous void can be estimated using the following equation [39,40]:

$$E_{inc} = (E/p)_{cr} \cdot p \left[1 + B \cdot (p \cdot d)^{-n} \right] \quad (1)$$

where:

E_{inc} —PD inception field strength, $V \cdot m^{-1}$;

$(E/p)_{cr}$ —critical electric field to pressure ratio, for air 25.2 [$V \cdot m^{-1} \cdot Pa^{-1}$];

p —gas pressure in void [Pa];

d —gaseous void dimension (the void diameter or height parallel to the applied E field) [m];

B, n —ionization process coefficients (for air $B = 8.6 [m^{1/2} \cdot Pa^{1/2}]$, $n = 0.5$).

Figure 1 shows the curves of the PD inception field strength E_{inc} as a function of the dimension of the gaseous void d , estimated for air at different temperatures (from 4 °C to 90 °C). The reduction in the dimension of the gaseous void enclosed in the dielectric is accompanied by an increase in the value of the E field strength required for PD inception.

When the size of the void is reduced from 1.0 mm to 10 μm (i.e., 100 times), the PD inception field strength increases about 5 times. As can be seen in Figure 1, an increase in temperature also increases the value of the PD inception field strength. Due to the properties of gases, for an un-vented void of constant volume, $p/T = \text{const.}$, an increase in temperature causes a proportional increase in pressure and, consequently, also E_{inc} value. Both of the phenomena mentioned above (the effect of gaseous void dimension and gas temperature on E_{inc}) are of key importance for the analysis of the conditions for the formation of PD pulses in insulation defects of a current-carrying HVDC cable.

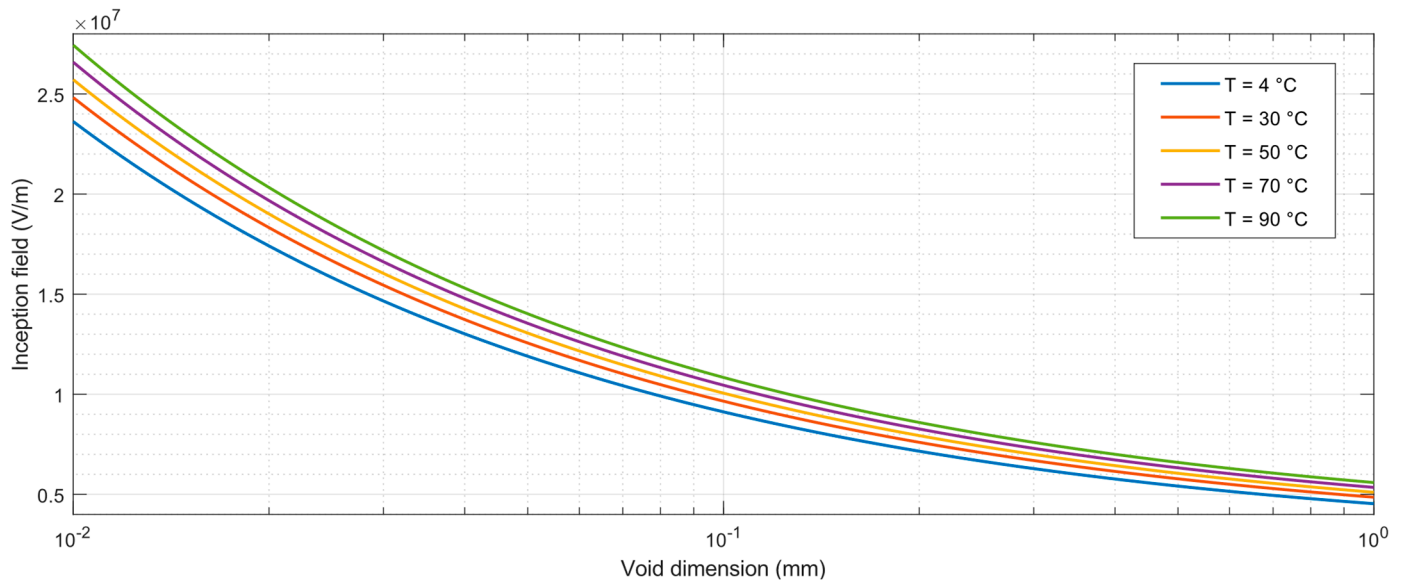


Figure 1. PD inception field vs. void dimension for different temperatures, from 4 °C up to 90 °C.

Fulfillment of the second condition necessary for PD inception requires the presence of a starting electron triggering the discharge development process. Due to the stochastic nature of the appearance of such an electron, a probability function (usually exponential) is defined for the lag time of the discharge occurrence relative to the moment when the field strength in the void reaches the E_{inc} value. An overview of the functions proposed by various authors for free electron supply and discharge probability can be found in [40]. In the PD source model implemented in the presented simulations, the discharge probability P_d was estimated based on the formula:

$$P_d = \begin{cases} 1 - \exp\left(-\frac{\Delta t_{\text{inc}}}{\tau_{\text{lag}}}\right) & E_{\text{void}} \geq E_{\text{inc}} \\ 0 & E_{\text{void}} < E_{\text{inc}} \end{cases} \quad (2)$$

where:

E_{void} —electric field strength in a gaseous void, $\text{V}\cdot\text{m}^{-1}$;

τ_{lag} —PD inception lag time, s;

Δt_{inc} —the period of time counted from the moment when the field strength in the void E_{void} exceeded the E_{inc} , s.

The occurrence of PD inside a gas void does not result in a reduction of the field strength in the void to zero at the end of the discharge. Due to the not fully recognized conditions of PD extinction in a gaseous void enclosed in dielectric, various estimations of the PD extinction field strength E_{ext} were proposed in published works. One way is to define E_{ext} as a proportional part of the critical field strength [39,40,62–64]:

$$E_{\text{ext}} \approx \chi \cdot E_{\text{cr}} \quad (3)$$

where:

E_{ext} —the PD extinction field strength, $\text{V}\cdot\text{m}^{-1}$;
 E_{cr} —the critical field strength, $\text{V}\cdot\text{m}^{-1}$;
 χ —the PD extinction field coefficient, -.

The value of the χ coefficient may depend on the type of gas, the dielectric in which the void is enclosed and the processes on its surface, streamer polarization, temperature and field strength E inside the void, before the PD. Despite so many variable factors, approximate values of $\chi = 0.2$ for positive streamers and $\chi = 0.5$ for negative streamers [39,63] or their average value of $\chi = 0.35$ [64] are assumed for numerical PD simulations. An alternative method of estimating the value of E_{ext} is to assume a constant value of the residual field strength, which, based on various research studies, may be about $0.1 \text{ kV}\cdot\text{mm}^{-1}$ or about $1 \text{ kV}\cdot\text{mm}^{-1}$ [40].

2.2. Electric Field in Model HVDC Cable Insulation

HVDC cable usually has a complex, multi-layer coaxial construction. There is an electric field in the insulation of the energized cable, which is created between the semi-conductive screen on the cable core, with a high electric potential resulting from the applied voltage, and the semi-conductive screen on the insulation, which is at ground potential. The distribution of the DC electric field depends on the electrical conductivity σ of the dielectric. This material parameter of dielectrics is non-linearly dependent on temperature and electric field strength. To determine the distribution of the E field in the HVDC cable insulation, often an empirically determined function is used to estimate the value of electrical conductivity of a dielectric in specified conditions [42–45,48,51,55,57,59,60]:

$$\sigma(T, E) = \sigma_0 \cdot \exp(\alpha \cdot T) \cdot \exp(\beta \cdot E) \quad (4)$$

where:

σ_0 —specific dielectric conductivity, $\text{S}\cdot\text{m}^{-1}$ (at $E = 0.0 \text{ V}\cdot\text{m}^{-1}$ and $T = 0 \text{ }^\circ\text{C}$);
 T —temperature, $^\circ\text{C}$;
 E —electric field strength, $\text{V}\cdot\text{m}^{-1}$;
 α —temperature factor of conductivity, $^\circ\text{C}^{-1}$;
 β —field factor of conductivity, $\text{V}^{-1}\cdot\text{m}$.

Determining the appropriate values of coefficients α and β for numerical simulations may be a problem, because the published results of measurements performed for various XLPE samples show a large dispersion of their values. Reported values of the temperature factor of conductivity α range from $0.052 \text{ }^\circ\text{C}^{-1}$ to $0.180 \text{ }^\circ\text{C}^{-1}$ [45,65–67] and the variation of the field factor of conductivity β extends from $0.018 \times 10^{-6} \text{ V}^{-1}\cdot\text{m}$ to $0.5 \times 10^{-6} \text{ V}^{-1}\cdot\text{m}$ [65–67]. In addition, the measurements showed a dependence of β on temperature [66,67].

In order to take into account the influence of temperature and electric fields on conductivity in polymer insulation, a model function derived from the hopping theory of conduction in dielectrics is also often used [41,42,46,49,68–72]:

$$\sigma(T, E) = A \cdot \exp\left(\frac{-\varphi \cdot q_e}{k_B \cdot T}\right) \cdot \frac{\sinh|B|E|}{|E|} \quad (5)$$

where:

A, B —specific factors for the dielectric;
 φ —thermal activation energy, eV;
 q_e —elementary charge;
 T —temperature, K;
 E —electric field strength, $\text{V}\cdot\text{m}^{-1}$.

Electrical conductivity is highly sensitive to temperature changes and less sensitive to electric field strength changes. For this reason, the temperature field existing in the insulating material has a dominant influence on the distribution of the electric field. Joule

heat is produced in a cable conductor by the flow of operating, overload or fault current. This causes the temperature distribution in the insulation of the coaxial cable to be radial. For a loaded cable, the highest temperature is in the cable core and the lowest is at the outer shield. As a result, the inner layers of insulation, at the cable core, have a significantly higher conductivity than the outer layers. The increase in the conductivity of the inner layers of the dielectric material reduces the electric field stress in the vicinity of the cable core. For this reason, the high temperature of the core conductor can cause the inversion of the electric field strength distribution in the dielectric (in a radial direction). Then the electric field stress near the screen on the insulation may be higher than the stress near the cable core.

The second effect of the change in the radial temperature distribution in the insulation, caused by the heating of the cable core, is the modification of the PD inception field strength. An increase in gas temperature in a void of constant volume causes a proportional increase in pressure, which in turn leads to an increase in E_{inc} (see Section 2.1).

For numerical simulations of PD in HVDC cable insulation, a coupled electro-thermal 2D model was implemented in the COMSOL[®] program [73]. The model takes into account both mentioned effects of the temperature field influence on the conditions of PD formation in gaseous voids. The parameters of the model used for problem analysis take into account the individual properties of each material included in the layered structure of the HVDC cable with XLPE insulation.

In the numerical procedure of the electric field simulation used to determine the time sequence of the PD pulses, it was assumed that the test value of the DC voltage is not determined by a voltage step at the time $t = 0$ s, but is achieved by monotonically increasing the voltage at the cable core in accordance with the quarter-wave of the 50 Hz AC voltage from 0 V to peak value, i.e., during 5 ms. The initial distributions of the electric field and the space charge in the cable insulation are, therefore, determined mainly by the permittivity and the defined voltage transient at the cable core in relation to the outer shield on the insulation (i.e., between the inner and outer electrode of the concentric cable model). Space charges from other sources (e.g., trapped in the volume of insulating material) have not been modeled, so the transient processes of the E field and charge distributions occurring after the DC voltage is established are related to the influence of electrical conductivity, the value of which at a specific location on the cable radius depends on the temperature and electric field, according to Equation (4).

2.3. Cable Model for E Field Analysis with Finite Element Method

The objects of the numerical analysis were three models of the HVDC cables with XLPE insulation with rated voltages of 150 kV [65,73], 320 kV and 500 kV [53]. Due to the thickness of the XPLE insulation layer of each cable, the average electric field strength E_{avg} in the insulation is $18.75 \text{ kV}\cdot\text{mm}^{-1}$, $16.00 \text{ kV}\cdot\text{mm}^{-1}$ and $21.74 \text{ kV}\cdot\text{mm}^{-1}$, respectively.

A cross-section showing the multi-layer structure of the modeled cables is shown in Figure 2. Parameters of materials of subsequent layers, necessary for modeling thermal processes in the cable and the temperature field in XLPE insulation, are listed in Table 1. The geometric dimensions of the layers for each of the analyzed cables are defined in Table 2, where the radii of individual layers are listed. The inner radius of the insulation layer is x_{min} and the outer radius is x_{max} (Figure 2, Table 2). Table 3 summarizes the general parameters defining the properties of XLPE insulation and the air filling the void, as well as the thermal parameters of the cable environment (laying the cable in water with a temperature of $4 \text{ }^\circ\text{C}$ is assumed). In the simulations, time sequences of PD pulses in two spherical voids with a diameter of 0.5 mm each were determined. In all three analyzed cable cases, the first void is located near the cable core (center of the gaseous void on the inner insulation radius +1 mm), and the second one near the grounded screen on the insulation (center of the gaseous void on the outer insulation radius –1 mm), Table 4.

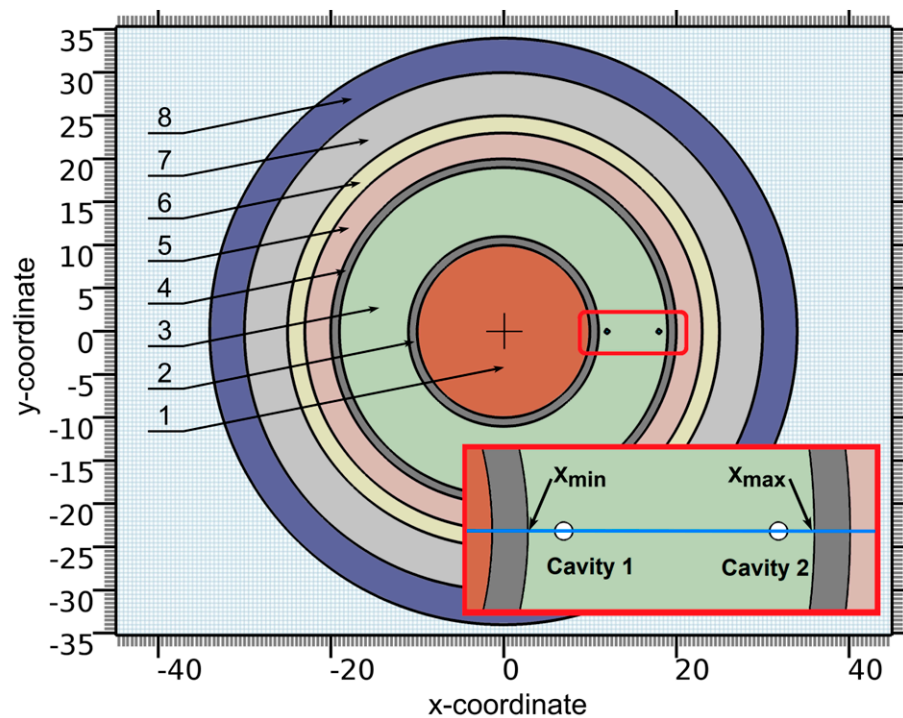


Figure 2. Geometry of HVDC cable model with two voids in XLPE insulation. Details of the insulation area with voids located on the cable radius (blue line) are shown in the red box. The cable layers are numbered according to their order in Tables 1 and 2.

Table 1. Parameters of materials for 150 kV, 320 kV and 500 kV cable models [65].

No	Cable Layer	k ($W \cdot m^{-1} \cdot K^{-1}$)	C_p ($J \cdot kg^{-1} \cdot K^{-1}$)	ρ ($kg \cdot m^{-3}$)
1	Core conductor	385	384	8900
2	Semicon layer	0.23	2050	1100
3	Insulation (XLPE)	0.32	2250	920
4	Semicon layer	0.23	2050	1100
5	Lead sheath	0.21	125	11,340
6	PE sheath	0.40	2300	950
7	Armoring	260	2300	2700
8	Outer serving	0.30	2350	950

Table 2. Dimensions of layers for 150 kV, 320 kV and 500 kV cable models.

No	Cable Layer	150 kV Cable r (mm)	320 kV Cable r (mm)	500 kV Cable r (mm)
1	Core conductor	10	28.8	33.5
2	Semicon layer (x_{min})	11	30.9	36
3	Insulation (x_{max})	19	50.9	59
4	Semicon layer	20	52.9	60
5	Lead sheath	23	55.8	64.5
6	PE sheath	25	58.3	70.5
7	Armoring	30	63.3	75.5
8	Outer serving	34	67.3	79.5

Table 3. Basic simulation parameters for HVDC cable models.

Parameter	Value	Unit
Initial conductivity of XLPE, σ_0 [65]	5.4×10^{-16}	$S \cdot m^{-1}$
Temperature factor of XLPE conductivity, α [65]	0.064	$^{\circ}C^{-1}$
Field factor of XLPE conductivity, β [65]	6.7×10^{-8}	$V^{-1} \cdot m$
Conductivity of air in void [70,71]	10^{-16}	$S \cdot m^{-1}$
Conductivity of air in void during PD	10^{-3}	$S \cdot m^{-1}$
Dielectric constant of gas	1.0	-
Dielectric constant of XLPE	2.3	-
External heat transfer coefficient	30	$W \cdot m^{-2} \cdot K^{-1}$
External temperature	4	$^{\circ}C$

Table 4. Simulation parameters for 150 kV, 320 kV and 500 kV cable models.

Parameter	150 kV Cable	320 kV Cable	500 kV Cable
Applied voltage, kV	150	320	500
1st void diameter, mm	0.5	0.5	0.5
1st void center x -coordinate, mm	12	31.9	37
2nd void diameter, mm	0.5	0.5	0.5
2nd void center x -coordinate, mm	18	49.9	58

3. Simulation Results—Case Studies for Three Model Cables

Figures 3–8 present, in the form of graphs, the results of the subsequent stages of the analysis of the conditions of the formation of PD pulses in the defined gaseous voids of three model HVDC cables. Distribution analyses of individual physical quantities were performed for thermal steady states at five different temperatures of the cable core: 4 °C, 30 °C, 50 °C, 70 °C and 90 °C. Figure 3 summarizes the temperature distributions in the insulation of individual cable models, which are the basis for the subsequent analyses.

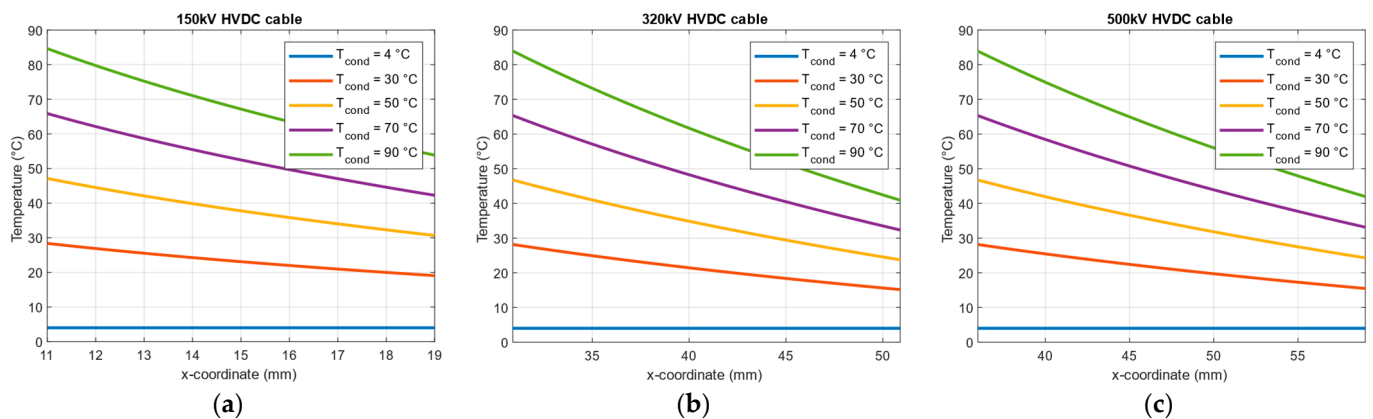


Figure 3. Distribution of temperature $T(x)$ across the cable insulation at 4 °C, 30 °C, 50 °C, 70 °C and 90 °C cable core temperatures for: (a) 150 kV HVDC cable; (b) 320 kV HVDC cable; (c) 500 kV HVDC cable.

The data visualized in Figure 4 shows the distributions of electrical conductivity in XLPE insulation on the radius of each of the cable models. The influence of temperature T and E field on conductivity σ was taken into account according to Equation (4), using the parameter values specified in Table 3.

Taking into account temperature distributions in the insulation of each cable model, simulations of E field strength distributions were carried out for a wide range of cable core temperatures (from 4 °C to 90 °C). As a result, distributions of the E field in cable insulation without voids were determined as a function of the x -coordinate on the radius

of the cable and the temperature of the cable core (Figure 5). For all three 2D distributions, cross-sections for five selected temperatures were separated, showing the corresponding reference distributions of the E field as a function of the x -coordinate (Figure 6).

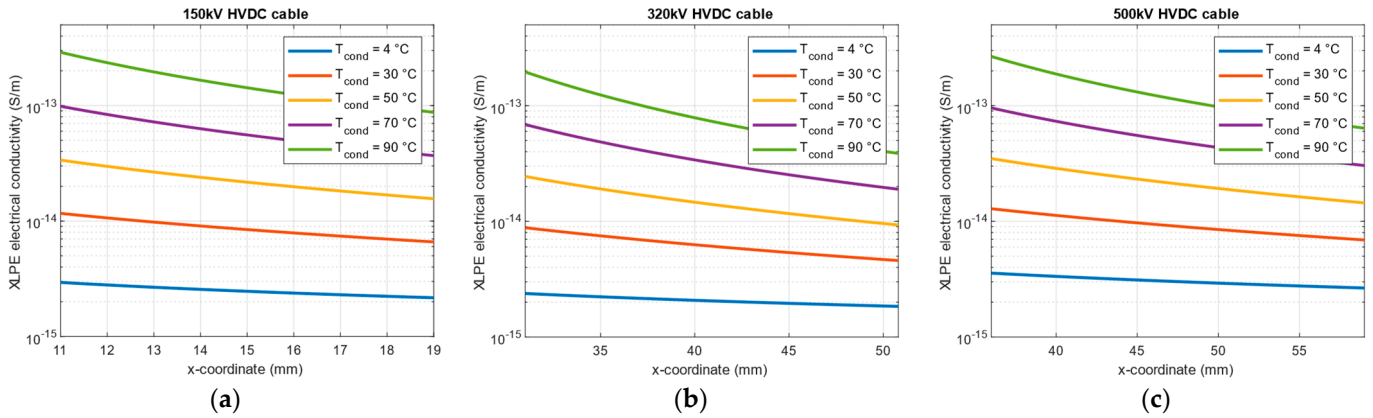


Figure 4. Distribution of electrical conductivity $\sigma(x)$ across the cable insulation at 4 °C, 30 °C, 50 °C, 70 °C, 90 °C cable core temperatures for: (a) 150 kV HVDC cable; (b) 320 kV HVDC cable; (c) 500 kV HVDC cable.

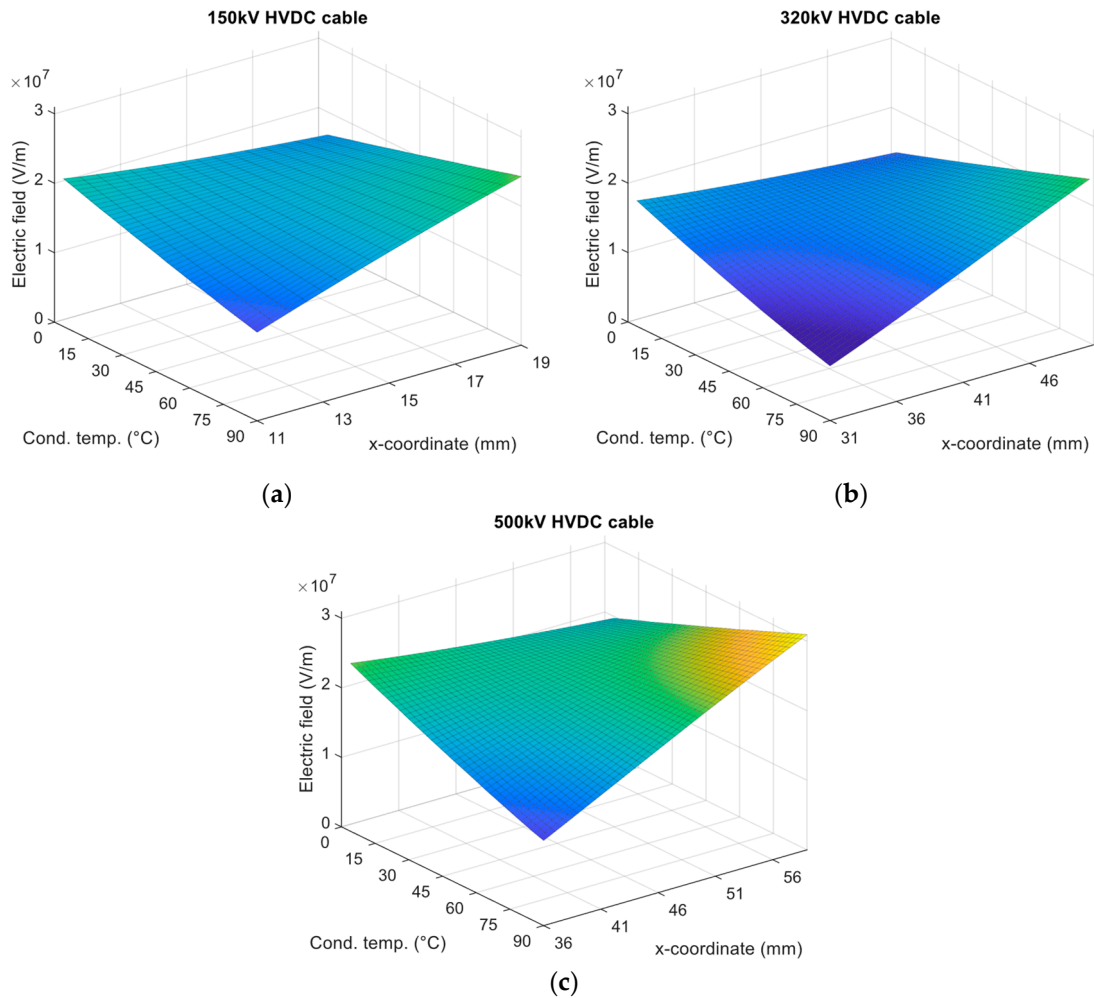


Figure 5. A 2D electric field distribution across the cable insulation at 4 °C to 90 °C cable conductor temperatures: (a) 150 kV HVDC cable; (b) 320 kV HVDC cable; (c) 500 kV HVDC cable.

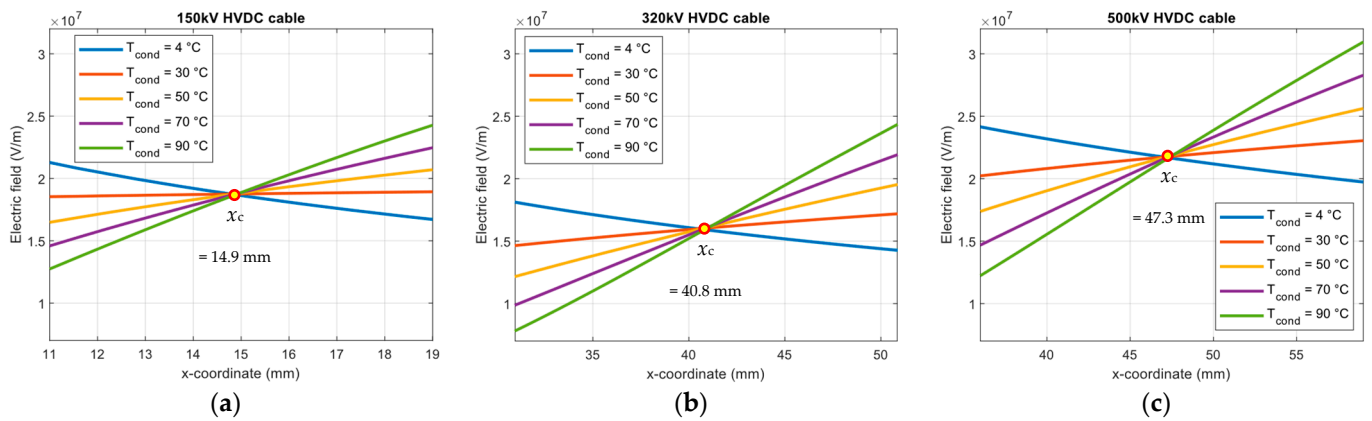


Figure 6. Electric field strength distribution $E(x)$ across the insulation at cable core temperatures of 4 °C to 90 °C: (a) 150 kV HVDC cable; (b) 320 kV HVDC cable; (c) 500 kV HVDC cable. At the x_c coordinate, the electric field strength E is almost constant.

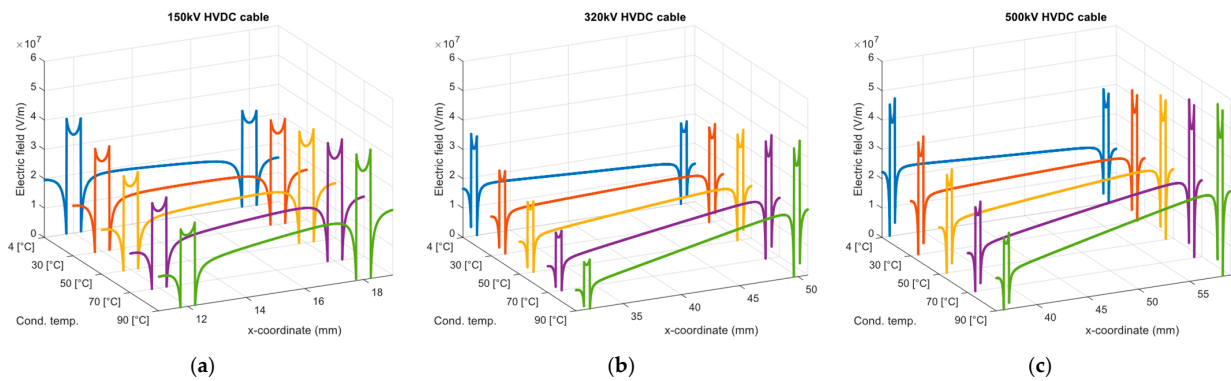


Figure 7. E field strength distribution in the cable insulation with two cavities at 4 °C, 30 °C, 50 °C, 70 °C and 90 °C conductor temperatures: (a) 150 kV HVDC cable; (b) 320 kV HVDC cable; (c) 500 kV HVDC cable. (Effects related to the formation of PD in the void have not been taken into account).

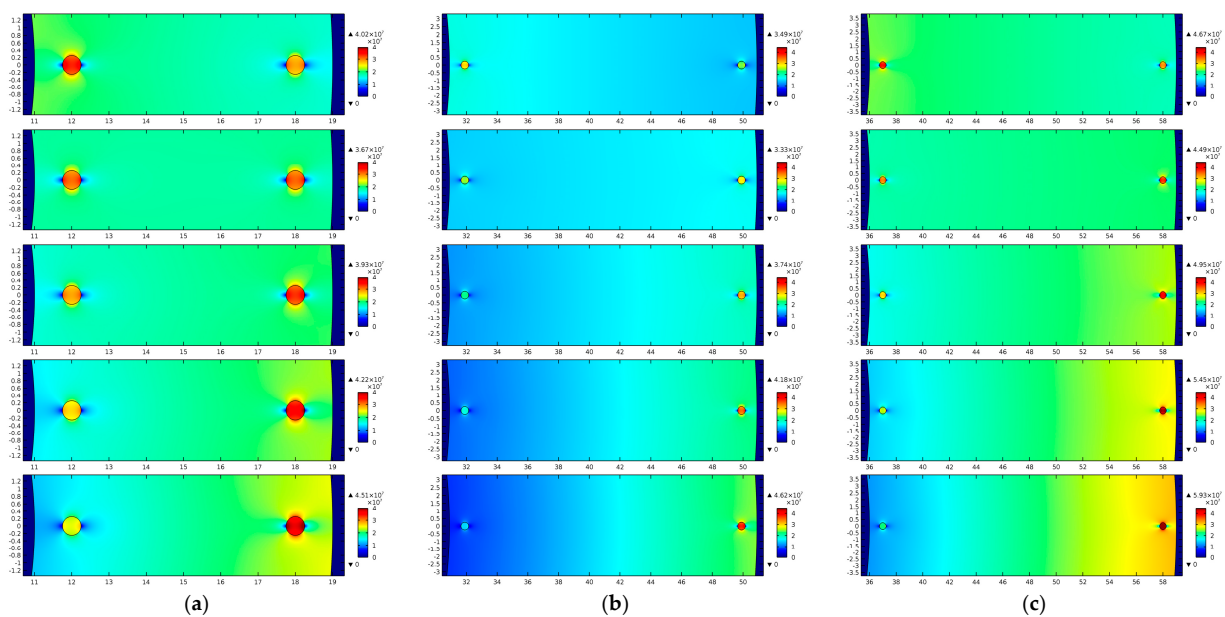


Figure 8. E field strength distribution in cable insulation with two cavities at 4 °C, 30 °C, 50 °C, 70 °C, 90 °C conductor temperature: (a) 150 kV HVDC cable; (b) 320 kV HVDC cable; (c) 500 kV HVDC cable. (Effects related to the formation of PD in the void have not been taken into account).

On the basis of numerically determined distributions of $T(x)$, $\sigma(x)$ and $E(x)$ for each cable, the values of these variables were determined for the boundary values of x coordinate, i.e., boundary temperatures (Table 5), boundary electrical conductivity (Table 6) and boundary E field strength in insulation without voids (Table 7). In addition, the conductance increase factor k_{σ} was defined as a ratio of the $\sigma_{x_{\min}}$ to $\sigma_{x_{\max}}$ (Table 6), and the differences ΔE between the E field strength at x_{\min} and x_{\max} coordinates (Table 7) were calculated. A negative value of ΔE means that the electric field inversion effect has occurred in insulation.

Table 5. Boundary temperatures in insulation of 150 kV, 320 kV and 500 kV cable models.

Cable Core Temperature	150 kV Cable			320 kV Cable			500 kV Cable		
	$T_{x_{\min}}, ^\circ\text{C}$	$T_{x_{\max}}, ^\circ\text{C}$	$\Delta T, ^\circ\text{C}$	$T_{x_{\min}}, ^\circ\text{C}$	$T_{x_{\max}}, ^\circ\text{C}$	$\Delta T, ^\circ\text{C}$	$T_{x_{\min}}, ^\circ\text{C}$	$T_{x_{\max}}, ^\circ\text{C}$	$\Delta T, ^\circ\text{C}$
4 °C	4.0	4.0	0.0	4.0	4.0	0.0	4.0	4.0	0.0
30 °C	28.4	19.1	9.3	28.2	15.2	13.0	28.2	15.5	12.7
50 °C	47.1	30.7	16.4	46.7	23.8	22.9	46.7	24.3	22.4
70 °C	65.9	42.3	23.6	65.3	32.3	33.0	65.3	33.1	32.2
90 °C	84.6	53.9	30.7	83.9	40.9	43.0	83.9	42.0	41.9

Table 6. Boundary electrical conductivity of insulation for 150 kV, 320 kV and 500 kV cable models.

Cable Core Temperature	150 kV Cable			320 kV Cable			500 kV Cable		
	$\sigma_{x_{\min}}, \text{S}\cdot\text{m}^{-1}$	$\sigma_{x_{\max}}, \text{S}\cdot\text{m}^{-1}$	$k_{\sigma}, -$	$\sigma_{x_{\min}}, \text{S}\cdot\text{m}^{-1}$	$\sigma_{x_{\max}}, \text{S}\cdot\text{m}^{-1}$	$k_{\sigma}, -$	$\sigma_{x_{\min}}, \text{S}\cdot\text{m}^{-1}$	$\sigma_{x_{\max}}, \text{S}\cdot\text{m}^{-1}$	$k_{\sigma}, -$
4 °C	2.9×10^{-15}	2.2×10^{-15}	1.32	2.4×10^{-15}	1.8×10^{-15}	1.33	3.6×10^{-15}	2.7×10^{-15}	1.33
30 °C	1.2×10^{-14}	6.6×10^{-15}	1.82	8.8×10^{-15}	4.6×10^{-15}	1.91	1.3×10^{-14}	6.9×10^{-15}	1.88
50 °C	3.4×10^{-14}	1.6×10^{-14}	2.13	2.5×10^{-14}	9.3×10^{-15}	2.69	3.5×10^{-14}	1.4×10^{-14}	2.50
70 °C	9.9×10^{-14}	3.7×10^{-14}	2.68	6.9×10^{-14}	1.9×10^{-14}	3.63	9.6×10^{-14}	3.0×10^{-14}	3.20
90 °C	2.9×10^{-13}	8.7×10^{-14}	3.33	2.0×10^{-13}	3.9×10^{-14}	5.13	2.7×10^{-13}	6.4×10^{-14}	4.22

Table 7. Boundary E field strength in insulation of 150 kV, 320 kV and 500 kV cable models.

Cable Core Temperature	150 kV Cable			320 kV Cable			500 kV Cable		
	$E_{x_{\min}}, \text{kV}\cdot\text{mm}^{-1}$	$E_{x_{\max}}, \text{kV}\cdot\text{mm}^{-1}$	$\Delta E, \text{kV}\cdot\text{mm}^{-1}$	$E_{x_{\min}}, \text{kV}\cdot\text{mm}^{-1}$	$E_{x_{\max}}, \text{kV}\cdot\text{mm}^{-1}$	$\Delta E, \text{kV}\cdot\text{mm}^{-1}$	$E_{x_{\min}}, \text{kV}\cdot\text{mm}^{-1}$	$E_{x_{\max}}, \text{kV}\cdot\text{mm}^{-1}$	$\Delta E, \text{kV}\cdot\text{mm}^{-1}$
4 °C	21.3	16.7	4.6	18.1	14.3	3.8	24.2	19.7	4.5
30 °C	18.5	18.9	-0.4	14.6	17.2	-2.6	20.2	23.0	-2.8
50 °C	16.5	20.7	-4.2	12.1	19.5	-7.4	17.4	25.6	-8.2
70 °C	14.6	22.5	-7.9	9.9	21.9	-12.0	14.7	28.3	-13.6
90 °C	12.7	24.3	-11.6	7.8	24.4	-16.6	12.2	30.9	-18.7

In the next step of the analysis, the E field strength distributions were determined on the radius of each of the model cables with the presence of spherical gaseous voids, with the dimensions and locations described in Table 4. The indicated results of the simulation of E field strength distributions vs. the x -coordinate are presented in Figure 7. The scale of the E field axis is identical in all three sub-figures, while the scale of the x -coordinate axis is adapted to the geometry of each analyzed cable. It should be noted that these E_{void} simulations do not take into account that the highest field strength in the void is limited by the PD generation process.

The last stage of the static analyses was to determine the 2D distributions of the E field strength in the insulation of each of the model cables, in the areas where spherical gaseous voids were located (Figure 8). The E field strength (expressed in V/m) was color-coded with a scale from ‘cold’ (lowest E field value) to ‘hot’ (highest E field value). The E_{void} values for both voids and the E_{cable} in XLPE for the same two radii were tabulated and field enhancement factor ($FEF = E_{\text{void}}/E_{\text{cable}}$) values were calculated (Table 8).

Table 8. E field in void and in XLPE simulation results for 150 kV, 320 kV and 500 kV cable models.

Cable Core Temperature	150 kV Cable						320 kV Cable						500 kV Cable					
	1st Void			2nd Void			1st Void			2nd Void			1st Void			2nd Void		
	E_{void} kV·mm ⁻¹	E_{cable} kV·mm ⁻¹	FEF	E_{void} kV·mm ⁻¹	E_{cable} kV·mm ⁻¹	FEF	E_{void} kV·mm ⁻¹	E_{cable} kV·mm ⁻¹	FEF	E_{void} kV·mm ⁻¹	E_{cable} kV·mm ⁻¹	FEF	E_{void} kV·mm ⁻¹	E_{cable} kV·mm ⁻¹	FEF	E_{void} kV·mm ⁻¹	E_{cable} kV·mm ⁻¹	FEF
4 °C	33.6	20.5	1.64	28.5	17.2	1.66	29.7	17.8	1.67	24.4	14.4	1.69	38.6	23.9	1.62	32.7	19.4	1.69
30 °C	30.7	18.6	1.65	31.2	18.9	1.65	25.0	14.8	1.69	28.5	17.1	1.67	33.5	20.4	1.64	37.3	22.9	1.63
50 °C	28.5	17.1	1.67	33.0	20.2	1.63	21.6	12.6	1.71	31.6	19.3	1.64	29.7	17.8	1.67	40.7	25.3	1.61
70 °C	26.3	15.8	1.66	35.0	21.6	1.62	18.2	10.5	1.73	34.7	21.4	1.62	25.9	15.3	1.69	44.1	27.8	1.59
90 °C	24.4	14.4	1.69	37.1	23.0	1.61	15.1	8.6	1.76	37.9	23.6	1.61	22.4	13.1	1.71	47.4	30.2	1.57

The red color indicates the highest and blue the lowest values of the E field strength in each pair of gaseous voids (1st or 2nd), or in the dielectric at void x -coordinates, or value of the FEF . The green color indicates nearly equal E field values in pairs of voids.

The radial temperature distribution existing in the insulation of the HVDC cable causes the intensity of the PD inception field in the gaseous void, depending on the location of the void on the radius of the cable. Assuming that the gas temperature in the void is equal to the temperature of the surrounding dielectric, the values of E_{inc} vs. x -coordinate were determined for the selected cable core temperatures of each cable (Figure 9). Using a dedicated numerical procedure implemented in the MATLAB® program, sequences of successive distributions of the E field strength were generated for the electro-thermal model of the cable simulated in the COMSOL® program [73]. The general procedure of PD simulation is presented in Figure 10. The first step is creating a geometric model, setting the materials and physical parameters, establishing boundary settings and meshing. Next, electric and thermal computation vs. time is performed. During the simulation, the PD initiation condition is checked. Discharge can occur when the electric field strength in the void exceeds the value of the PD inception field, Equation (1). Moreover, the stochastic nature of PD generation is modeled using Equation (2). Discharge probability P_d is calculated and compared with random number R between 0 and 1. If $P_d > R$, the PD initiation conditions are met. Partial discharge development is simulated by increasing the conductivity of the gas in the void from 10^{-16} S·m⁻¹ to 10^{-3} S·m⁻¹. The flowing charge causes a decrease in the electric field inside the void. When the electric field in the gaseous void is reduced to the PD extinction field E_{ext} , discharge ends and the gas conductivity is reset to 10^{-16} S·m⁻¹. Individual PD charge is determined by integrating the current flowing through the void during discharge process. The entire procedure is repeated until the assumed simulation time is reached. In each simulation, the procedure was started 2000 s after applying the DC voltage.

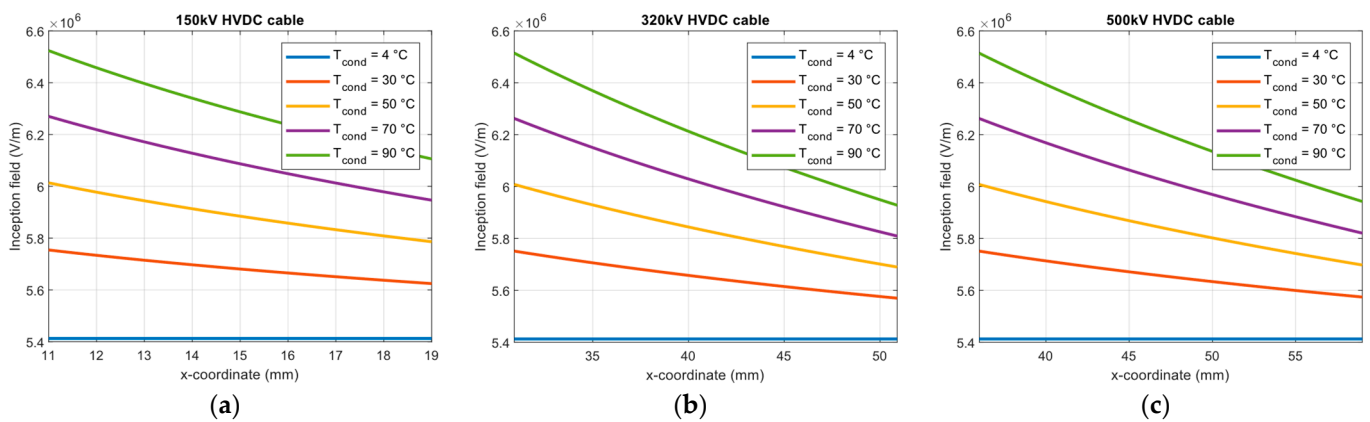


Figure 9. PD inception field in void of 0.5 mm diameter located in XLPE insulation of HVDC cable at 4 °C, 30 °C, 50 °C, 70 °C and 90 °C cable core temperatures for: (a) 150 kV HVDC cable; (b) 320 kV HVDC cable; (c) 500 kV HVDC cable.

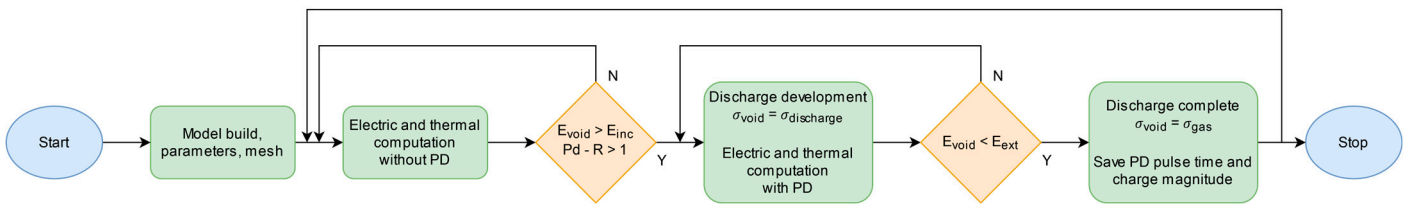


Figure 10. Block diagram of numerical procedure for determination of PD pulses generated in gaseous void in modeled HVDC cable insulation.

Effects related to the formation of PD pulses in both gaseous voids at field strengths reaching their individual E_{inc} values were taken into account. The time sequences of the PD pulses simulated in this way are shown in Figure 11.

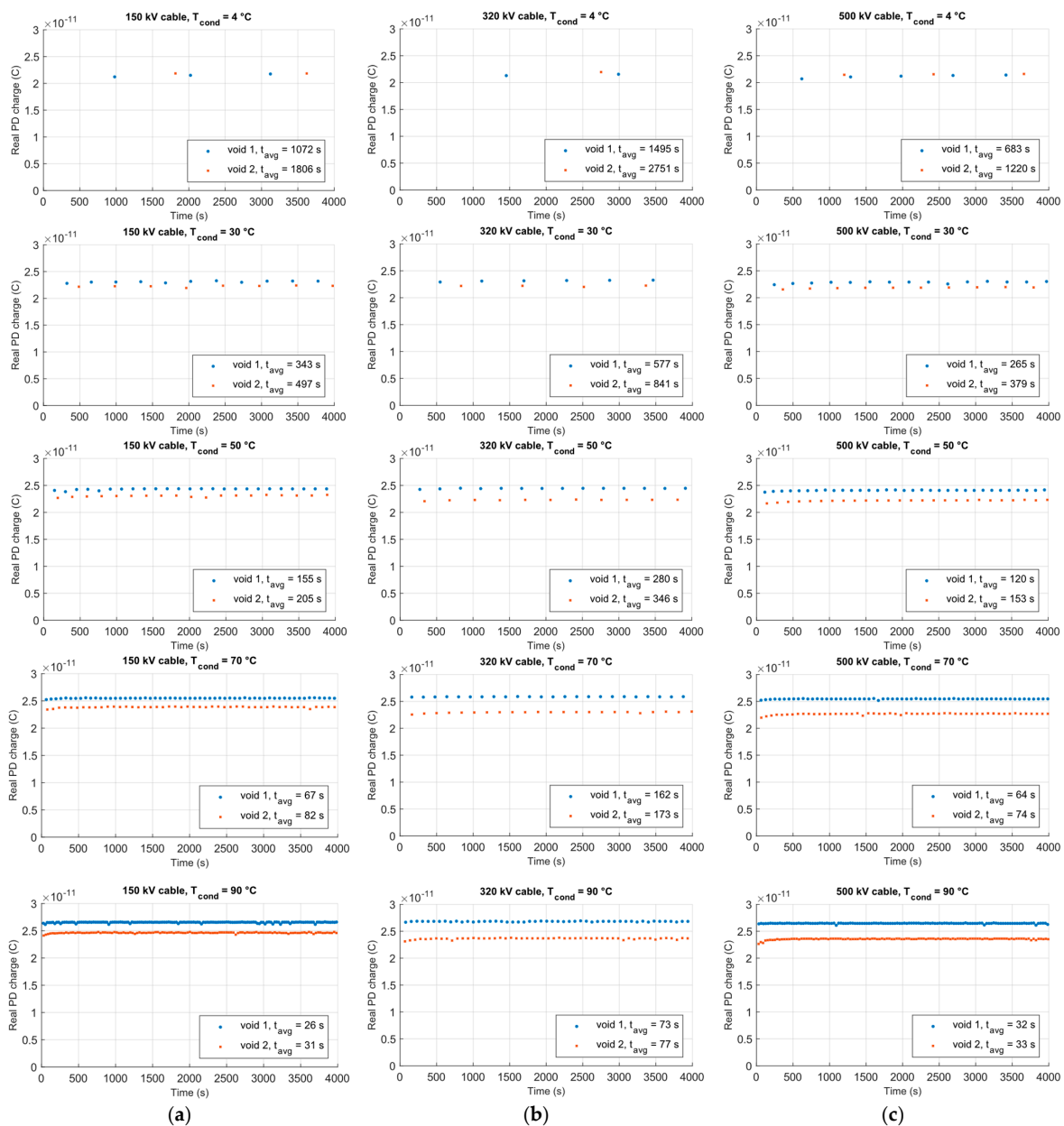


Figure 11. Simulated PD pulse sequences vs. time at 4 °C, 30 °C, 50 °C, 70 °C and 90 °C cable core temperatures for: (a) 150 kV HVDC cable; (b) 320 kV HVDC cable; (c) 500 kV HVDC cable.

The observed sequence of PD pulses in the cable insulation is the result of two independent discharge generation processes arising in the first and second gaseous voids (Figure 11). For each modeled cable (150 kV, 320 kV and 500 kV) and for selected cable core temperatures (4 °C, 30 °C, 50 °C, 70 °C and 90 °C) based on the simulated PD sequences, two basic statistical parameters were determined, characterizing the PD pulses at DC voltage (Table 9):

- Average PD magnitude q_{av} , pC;
- Average time interval between successive PD pulses Δt_{av} , s.

Table 9. Average PD charge q_{av} and average PD pulse time interval Δt_{av} for 150 kV, 320 kV and 500 kV cable models at selected cable core temperatures.

Cable Core Temperature	150 kV Cable				320 kV Cable				500 kV Cable			
	1st Void		2nd Void		1st Void		2nd Void		1st Void		2nd Void	
	q_{av} pC	Δt_{av} s										
4 °C	21.6	1072	21.8	1806	21.4	1495	21.9	2751	21.1	683	21.5	1220
30 °C	23.1	343	22.3	497	23.1	577	22.1	841	22.8	265	21.8	379
50 °C	24.3	155	23.1	205	24.4	280	22.3	346	24.1	120	22.2	153
70 °C	25.5	67	23.9	82	25.9	162	22.9	173	25.4	64	22.7	74
90 °C	26.5	26	24.6	31	26.8	73	23.6	77	26.5	32	23.6	33

4. Discussion

The presented results of thermal and electric field analyses for models of three HVDC cables with different rated voltages (150 kV, 320 kV and 500 kV), different surface areas of the cable core (300 mm², 2500 mm² and 3000 mm²) and different structures of the outer layers covering the XLPE insulation are the basis for determining the conditions for the formation of PD pulses in internal gaseous voids.

The electric field in the insulation of the HVDC cable, due to the direct dependence on the electrical conductivity of the insulating material, is a field coupled (indirectly) with the thermal field present in the volume of the cable insulation. For current-carrying cables with a concentric design, the resulting radial temperature distribution in the cable also modifies radially the conductivity of the insulation material. This leads to a significant increase in the electrical conductivity of the dielectric along the radius of the cable, from the lowest conductivity at the outer radius of the insulation to the highest at the inner radius of the insulation (i.e., near the cable core with the highest temperature). Moreover, according to Equation (4) or (5), the conductivity of the dielectric is modified, also radially, by the presence of a DC electric field, which is influenced by the space charge present in the insulation volume. If the cable insulation is a modern XLPE polymer dedicated to HVDC applications (DC-XLPE), then the additional component of the E field produced by the space charge in steady state, a long time after applying a DC voltage, has a small value, even below 5% [54]. It follows that in such a state, the presence of space charge will only slightly affect the repetition rate of the PD pulses. However, the nature and trends of changes in PD parameters under the influence of the radial thermal field will be the same.

When estimating the conditions for the generation of the PD pulse sequence, the presence of a space charge in the insulation from sources other than the charge resulting from the application of the test voltage was not considered. More complex simulations may also take into account other charges present in the polymer structure, e.g., related to the presence of polar additives or impurities [74].

For the numerical simulations of steady states of the coupled thermo-electric field, performed in the COMSOL Multiphysics[®] 6.0 program, a constant value of the temperature of the external environment of the cable (4 °C) was assumed, while the temperature of the cable core was the modified parameter (from 4 °C to 90 °C). Obviously, for all three

cables, similar insulation temperatures were obtained at the inner radius of the insulation x_{\min} for each core temperature and the calculated differences are not greater than $0.7\text{ }^{\circ}\text{C}$ for a conductor temperature of $90\text{ }^{\circ}\text{C}$ (Figure 3 and Table 5). Due to the thickness of the XLPE insulation and the structure of the outer layers of the cables, the smallest decrease in temperature occurs in the insulation of the 150 kV cable, and the largest in the 320 kV cable. For example, when the temperature of the conductor is $70\text{ }^{\circ}\text{C}$, then the numerically estimated temperature differences for the inner and outer radius of insulation for the mentioned cables are $23.6\text{ }^{\circ}\text{C}$ and $33\text{ }^{\circ}\text{C}$, respectively (Table 5). This fact has consequences for the conductivity distribution (Figure 4) and electric field strength (Figures 5 and 6) observed along the x -coordinate in the cable insulation. Already, at a conductor temperature of $30\text{ }^{\circ}\text{C}$, the electric field inversion effect occurs. The full ranges of variation of electric field strength E , caused by a change in conductor temperature, are:

- (a) On the inner radius of the insulation x_{\min}
 - For 150 kV cable, from $12.7\text{ kV}\cdot\text{mm}^{-1}$ to $21.3\text{ kV}\cdot\text{mm}^{-1}$;
 - For 320 kV cable, from $7.8\text{ kV}\cdot\text{mm}^{-1}$ to $18.1\text{ kV}\cdot\text{mm}^{-1}$;
 - For 500 kV cable, from $12.2\text{ kV}\cdot\text{mm}^{-1}$ to $24.2\text{ kV}\cdot\text{mm}^{-1}$.
- (b) On the outer radius of the insulation
 - For 150 kV cable, from $16.7\text{ kV}\cdot\text{mm}^{-1}$ to $24.3\text{ kV}\cdot\text{mm}^{-1}$;
 - For 320 kV cable, from $14.3\text{ kV}\cdot\text{mm}^{-1}$ to $24.4\text{ kV}\cdot\text{mm}^{-1}$;
 - For 500 kV cable, from $19.7\text{ kV}\cdot\text{mm}^{-1}$ to $30.9\text{ kV}\cdot\text{mm}^{-1}$.

Taking into account the above data, and Equation (1) and the data contained in Figure 1, it should be noted that the distributions of the field strength E for the cable model with two gaseous voids, presented in Figures 7 and 8, are not adequate to the real situation in the modeled cables. These distributions were only used to estimate the FEF values for the analyzed gaseous voids. The FEF values, obtained as a result of numerical simulations, ranging from 1.62 to 1.76 for all considered cases, are in good agreement with the results obtained in the 2D simulations presented in [71]. According to this paper, the more accurate results obtained from the 3D simulation are about 16% lower.

Due to the very high values of the DC field strength in the insulation of all three analyzed model cables (Figure 6), a 0.5 mm spherical gas void will be the source of PD in each of the considered cases (Figure 9). Of course, any gaseous void large enough to have a PD inception field strength (Figure 1) lower than the estimated electric field strength inside the void will be a potential PD source. This is a problem that is related to the influence of micro-defects of the XLPE polymer structure (with dimensions below $30\text{ }\mu\text{m}$) on the rate of damage growth and the estimated lifetime of the insulation [37,38]. If the radial distributions of the electric field in HVDC cables (Figure 6) are related to the estimated values of the PD inception field E_{inc} as a function of the dimension d of the gaseous void (Figure 1; curves $E_{\text{inc}} = f(d)$, parameterized by the gas temperature), then it is possible to estimate the critical dimension d_{cr} of the gaseous void (i.e., the minimum void size for which PD can arise for local electro-thermal field conditions) vs. the location of the gaseous void on the radius of the cable. Figure 12 compares the results of the d_{cr} estimation for the three analyzed HVDC cables. For these calculations, a simplifying assumption was made that for each gaseous void, the field enhancement factor FEF is 1.65 (see Table 8).

The results of the estimation of the critical dimension d_{cr} (Figure 12) indicate that for 150 kV and 500 kV cables in the full range of the analyzed temperatures, they are lower than $20\text{ }\mu\text{m}$, and for the 320 kV cable only for the highest temperatures and x -coordinates close to the cable core are they are greater than this value. Three decades ago, the size of a gaseous void of $20\text{ }\mu\text{m}$ was the quality control level for defects of this type in the XLPE insulation of 500 kV cables [75]. Analyses of XLPE insulation lifetime models have shown, however, that the estimated critical sizes of microstructural defects are one order of magnitude smaller [37,38,51]. Damage to the cross-linked structure of XLPE at the microvoid–polymer interface caused by effective hot electrons may, under conditions of strong field stress, lead to the initiation of the electric treeing process and, as a result, shorten the life of the

insulation [38,51]. The performed numerical simulations show that for 150 kV and 500 kV cables in a wide range of x -coordinates, and for a 320 kV cable in a narrower range, PD inception can occur in voids with dimensions of several micrometers, below 10 μm and down to 2 μm .

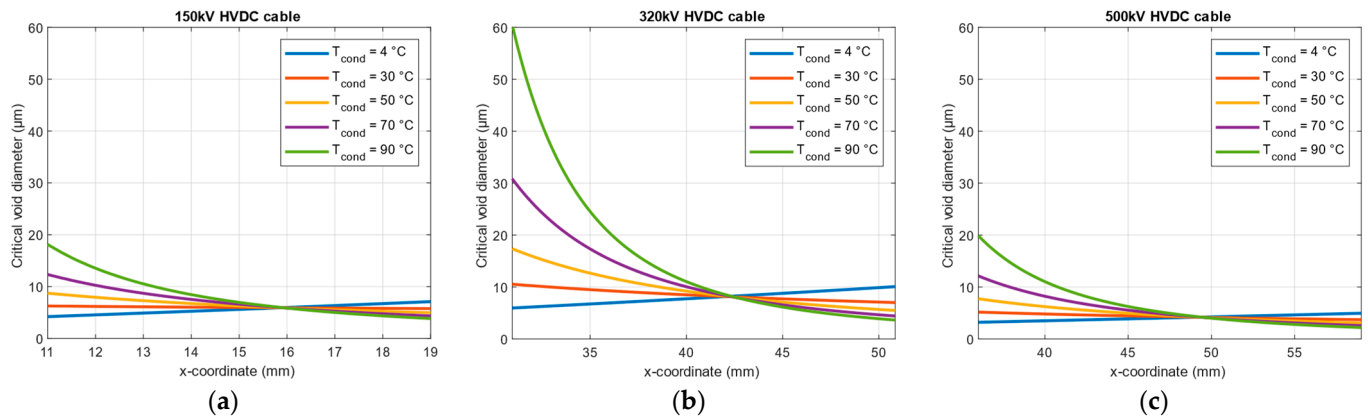


Figure 12. Critical diameter of gaseous void d_{cr} vs. x -coordinate in HVDC cable at 4 °C, 30 °C, 50 °C, 70 °C and 90 °C cable core temperatures for: (a) 150 kV HVDC cable; (b) 320 kV HVDC cable; (c) 500 kV HVDC cable.

The comparison of the results for all three cables shows that the design parameters, electrical and thermal, as well as the geometry of the cable have a significant impact on the critical dimension of the gaseous void. The 320 kV cable, with a more conservative design, has slightly lower electric field stress than the other two cables (Figures 5 and 6). For this reason, and due to the temperature field generated in the insulation of the loaded cable (Figure 3), this results in higher values of the critical dimension d_{cr} for this cable.

It should be noted that from the point of view of assessing the correctness and accuracy of simulation results carried out in the COMSOL[®] program, reducing the size of gaseous voids leads to a significant increase in the numerical complexity of the entire model and time-consuming calculations. High-resolution analysis of time sequences of PD pulses, generated in voids with sizes of the order of single micrometers, while taking into account the full geometry of the HVDC cable, requires the use of a computer hardware platform with very high computing performance and memory resources sufficient to allocate the extensive mesh model of the analyzed cable.

If the conditions necessary for PD inception are not met in a thermally stable model of cable insulation with a gaseous inclusion, the considered field problem is static. The presence of an active void in the insulation (i.e., one in which the conditions for the formation of PD are met) makes modeling a dynamic problem. The mechanism of discharge generation in the void is conditioned by the threshold value E_{inc} , exceeding which causes the creation of the PD pulse. Thus, a time-varying disturbance of the local electric field in the void and the dielectric around it is initiated. In circuit models, this corresponds to a short-term discharge of the void's electric capacitance and a slow process of its charging in a circuit with a long time constant. The parameters of the equivalent scheme elements of an insulating system with a void depend on the values of material constants (dielectric constant and resistivity/conductivity), which in turn are conditioned by temperature and electric field [39,76–78]. The magnitude of the PD from the void at a smooth DC voltage has a small dispersion compared to the PD at an AC voltage. When DC voltage ripple is present, then the PD charge dispersion is greater due to the influence of the statistically variable lag time.

In the HVDC cable model implemented by combining the functionality of MATLAB[®] and COMSOL[®], it was possible to determine the sequence of PD pulses generated in the analyzed gaseous voids. Considering the variable nature of the radial distribution of the E field in the insulation of the HVDC cable and the presence of a point with the coordinate

x_c , for which the E field is always almost constant (Figure 6), the insulation volume can be divided into two zones:

- Zone I, closer to the cable core, limited by x_{\min} and x_c radii;
- Zone II, closer to the outer screen on the insulation, limited by x_c and x_{\max} radii.

The relationship between the volume of cable insulation in Zone II and the insulation in Zone I can be defined by the formula:

$$k_V = 100 \frac{\text{Volume of Zone II}}{\text{Volume of Zone I}} = 100 \frac{x_{\max}^2 - x_c^2}{x_c^2 - x_{\min}^2} [\%] \quad (6)$$

where:

k_V —zone volume factor, %;

x_{\min} —inner radius of insulation, mm;

x_{\max} —outer radius of insulation, mm;

x_c —radius of the insulation layer with (almost) constant E field, mm.

For the three analyzed cable models (150 kV, 320 kV and 500 kV) the k_V values are 138%, 130% and 132%, respectively. Assuming that the distribution of defects in the insulation is uniform, more than 40% of the gaseous voids are exposed to the conditions characteristic of Zone I, and almost 60% to the conditions of Zone II. In an unloaded cable, the E field distribution is ‘normal’, i.e., it is similar to the distribution in an AC cable and the highest field stress occurs at the inner radius of the insulation. This is the reason for the shorter average time interval between successive PD pulses Δt_{av} in voids located near the cable core (Figure 10 and Table 9, conductor temperature 4 °C). The heating of the conductor and the creation of a radial thermal field causes an inversion of the E field distribution (Figures 5 and 6). Then, the complex electro-thermal stresses in both zones change, affecting the conditions of PD formation in gaseous voids. An increase in the gas temperature also causes an increase in the PD inception field strength, and thus an increase in the PD charge. This effect is more pronounced in the area near the cable core (Figure 10 and Table 9). At the same time, due to a significant increase in conductivity, the PD repetition rate increases, in particular in sources located in areas with the highest temperature, i.e., in Zone I, close to the cable core. A similar effect of changing the parameters of the PD pulse sequence was also obtained in other studies based on field modeling of the gaseous void in XLPE insulation of HVDC cables [70,72]; however, the influence of the location of the defect on the PD time sequences was not analyzed. It is seen that the factor increasing the PD repetition rate is also the E field strength, reaching for loaded cable the highest values in Zone II, especially in the area close to the outer radius of the insulation. The factors causing the increase of the PD repetition rate, i.e., increase of conductivity and increase of the E field strength, occur simultaneously, but in the heated cable their radial distributions are mutually inverse. For this reason, the observed effect of increasing the PD repetition rate in HVDC cable is the result of the synergistic effect of both of these factors.

5. Conclusions

The problem presented in the article concerns the conditions for the generation of PD pulses and their time sequences in the XLPE insulation of HVDC cable in steady state. Elements of research originality, including numerical simulations and analyses, cover several different aspects of this topic:

1. Reference of the conditions of PD formation in XLPE insulation of ‘cold’ and ‘hot’ HVDC cables to the location of the gaseous void on the cable radius; these analyses concerned three different designs of HVDC cables, but their results can be generalized;
2. Simulating and analyzing the parameters of the sequence of PD pulses generated independently in two PD sources with different locations on the cable radius;

3. Distinguishing two zones in the HVDC cable where the conditions of PD formation in the ‘cold’ and ‘hot’ cable insulation are different due to the radial temperature distribution and ‘normal’ or ‘inverted’ electric field distribution;
4. Estimation of the critical dimension of the gaseous void depending on the position and thermal condition of the cable insulation, for each of the analyzed projects.

The planned further extension of the analyses will take into account the effects related to the accumulation of space charge in the insulation bulk and at interfaces, as well as the increase of E field stress in transient states, including those resulting from voltage polarity reversal.

Table 10 summarizes the conditions for the formation of PD in the gaseous void and the basic characteristics of the PD pulses and their time sequences in both distinguished zones of the XLPE insulation of the HVDC cable (Zone I and Zone II).

Table 10. Characteristics of PD in two zones of HVDC cable insulation.

Insulation Zone	Unloaded Cable (‘Cold’)	Loaded Cable (‘Hot’)
Zone I	<p>Insulation temperature equal to environment temperature.</p> <p>Very low electrical conductivity of insulation material.</p> <p>Very high electric field stress, highest near inner insulation radius (as in an AC cable).</p> <p>Very low repetition rate of PD pulses, but for voids with identical parameters higher than in Zone II (influence of higher E field stress).</p> <p>PD charges as in Zone II, with a small dispersion of values. In the case of DC voltage ripple, there is a greater variability of the PD magnitude due to the influence of lag time.</p> <p>Due to the higher electric field strength, PD sources of smaller critical dimension than in Zone II may be also active.</p>	<p>High insulation temperature, the highest at the cable core.</p> <p>Higher electrical conductivity of the insulation material, highest near inner insulation radius.</p> <p>Significant reduction of electric field stress, lowest stress near inner insulation radius.</p> <p>Significantly higher repetition rate of PD pulses (several dozen times compared to a ‘cold’ cable), as a result of the combined action of higher temperature and increased E field stress.</p> <p>An increase in the PD magnitude (over a dozen percent), caused by an increase in E_{inc}, due to the higher gas pressure in the closed void.</p> <p>An increase in the temperature of the cable core increases the critical dimension of the void near the core.</p>
Zone II	<p>Insulation temperature equal to environment temperature.</p> <p>Very low electrical conductivity of insulation material.</p> <p>Reduced electric field stress, lower than in Zone I, lowest near the outer radius of the insulation (as in an AC cable).</p> <p>Very low repetition rate of PD pulses.</p> <p>PD charges as in Zone I, with a small dispersion of values. In the case of DC voltage ripple, there is a greater variability of the PD magnitude due to the influence of lag time.</p> <p>Critical dimension of the gaseous void slightly larger than in Zone I.</p>	<p>Increased insulation temperature, lowest on the outer radius of the insulation.</p> <p>Higher electrical conductivity of the insulation material, but lower than in Zone I; lowest on the outer radius of the insulation.</p> <p>Very high electric field stress, highest near outer insulation radius.</p> <p>Significantly higher repetition rate of PD pulses (several dozen times compared to a ‘cold’ cable), as a result of the combined action of higher temperature and increased E field stress.</p> <p>A slight increase in PD magnitude (several percent), caused by an increase in E_{inc}, due to the higher gas pressure in the closed void.</p> <p>The critical dimension of the gaseous void can be significantly smaller than in Zone I (depending on the temperature of the cable core).</p>

Author Contributions: Conceptualization, P.Z.; methodology, P.Z. and P.M.; software, P.M.; validation, P.Z. and P.M.; resources, P.Z. and P.M.; data curation, P.M. and P.Z.; writing—original draft preparation, P.Z. and P.M.; writing—review and editing, P.Z. and P.M.; visualization, P.M.; supervision, P.Z. All authors have read and agreed to the published version of the manuscript.

Funding: This research received no external funding.

Data Availability Statement: Not applicable.

Conflicts of Interest: The authors declare no conflict of interest.

References

1. Humpert, C. Long distance transmission systems for the future electricity supply—Analysis of possibilities and restrictions. *Energy* **2012**, *48*, 278–283. [[CrossRef](#)]
2. Hammons, T.J.; Lescale, V.F.; Uecker, K.; Haeusler, M.; Retzmann, D.; Staschus, K.; Lepy, S. State of the art in ultrahigh-voltage transmission. *Proc. IEEE* **2012**, *100*, 360–390. [[CrossRef](#)]
3. Zhou, H.; Qiu, W.; Sun, K.; Chen, J.; Deng, X.; Qian, F.; Wang, D.; Zhao, B.; Li, J.; Li, S.; et al. (Eds.) *Ultra-High Voltage AC/DC Power Transmission*; Springer: Berlin/Heidelberg, Germany, 2019.
4. Worzyk, T. *Submarine Power Cables Design, Installation, Repair, Environmental Aspects*; Springer: Berlin/Heidelberg, Germany, 2009.
5. Mazzanti, G.; Marzinotto, M. *Extruded Cables for High-Voltage Direct-Current Transmission: Advances in Research and Development*; Wiley-IEEE Press: Hoboken, NJ, USA, 2013.
6. Jovicic, D.; Ahmed, K. *High-Voltage Direct-Current Transmission. Converters, Systems and DC Grids*; John Wiley & Sons: Hoboken, NJ, USA, 2015.
7. Liu, R. Long-distance DC electrical power transmission. *IEEE Electr. Insul. Mag.* **2013**, *29*, 37–46. [[CrossRef](#)]
8. Alassi, A.; Bañales, S.; Ellabban, O.; Adam, G.; MacIver, C. HVDC transmission: Technology review, market trends and future outlook. *Renew. Sustain. Energy Rev.* **2019**, *112*, 530–554. [[CrossRef](#)]
9. Li, Z.; Song, Q.; An, F.; Zhao, B.; Yu, Z.; Zeng, R. Review on DC transmission systems for integrating large-scale offshore wind farms. *Energy Convers. Econ.* **2021**, *2*, 1–14. [[CrossRef](#)]
10. Acaroğlu, H.; Márquez, F.P.G. High voltage direct current systems through submarine cables for offshore wind farms: A life-cycle cost analysis with voltage source converters for bulk power transmission. *Energy* **2022**, *249*, 123713. [[CrossRef](#)]
11. ENTSO-E. *HVDC Links in System Operations, European Network of Transmission System Operators for Electricity*; Technical Paper; ENTSO-E: Brussels, Belgium, 2019.
12. Stan, A.; Costinaş, S.; Ion, G. Overview and assessment of HVDC current applications and future trends. *Energies* **2022**, *15*, 1193. [[CrossRef](#)]
13. Parol, M.; Robak, S.; Rokicki, Ł.; Wasilewski, J. Cable links designing in HVAC and HVDC submarine power grids—Selected issues. *Prz. Elektrotech.* **2019**, *95*, 7–13. [[CrossRef](#)]
14. Li, Y.; Liu, H.; Fan, X.; Tian, X. Engineering practices for the integration of large-scale renewable energy VSC-HVDC systems. *Glob. Energy Interconnect.* **2020**, *3*, 149–157. [[CrossRef](#)]
15. *Offshore Transmission Technology*; Report of ENTSO-E's Regional Group North Sea; European Network of Transmission System Operators for Electricity: Brussels, Belgium, 2011.
16. Stone, G.C.; Boulter, E.A.; Culbert, I.; Dhirani, H. *Electrical Insulation for Rotating Machines: Design, Evaluation, Aging, Testing, and Repair*, 1st ed.; Wiley-IEEE Press: Milwaukee, WI, USA, 2004.
17. *IEC 60505:2011*; Evaluation and Qualification of Electrical Insulation Systems. IEC: Genève, Switzerland, 2011.
18. Dissado, L.A.; Fothergill, J.C. *Electrical Degradation and Breakdown in Polymers*; Peregrinus Press: Chicago, IL, USA, 1992.
19. Jones, J.P.; Llewellyn, J.P.; Lewis, T.J. The contribution of field-induced morphological change to the electrical aging and breakdown of polyethylene. *IEEE Trans. Dielectr. Electr. Insul.* **2005**, *12*, 951–966. [[CrossRef](#)]
20. Marzinotto, M.; Mazzanti, G. The statistical enlargement law for HVDC cable lines part 1: Theory and application to the enlargement in length. *IEEE Trans. Dielectr. Electr. Insul.* **2015**, *22*, 192–201. [[CrossRef](#)]
21. Montanari, G.C.; Seri, P.; Dissado, L.A. Aging mechanisms of polymeric materials under DC electrical stress: A new approach and similarities to mechanical aging. *IEEE Trans. Dielectr. Electr. Insul.* **2019**, *26*, 634–641. [[CrossRef](#)]
22. Montanari, G.C.; Morshuis, P.; Seri, P.; Ghosh, R. Ageing and reliability of electrical insulation: The risk of hybrid AC/DC grids. *High Volt.* **2020**, *5*, 620–627. [[CrossRef](#)]
23. Naderiallaf, H.; Seri, P.; Montanari, G.C. Designing a HVDC insulation system to endure electrical and thermal stresses under operation. Part I: Partial discharge magnitude and repetition rate during transients and in DC steady state. *IEEE Access* **2021**, *9*, 35730–35739. [[CrossRef](#)]
24. Cambareri, P.; de Falco, C.; Rienzo, L.D.; Seri, P.; Montanari, G.C. Electric field calculation during voltage transients in HVDC cables: Contribution of polarization processes. *IEEE Trans. Power Deliv.* **2022**, *37*, 5425–5432. [[CrossRef](#)]
25. Lei, Z.; Song, J.; Tian, M.; Cui, X.; Li, C.; Wen, M. Partial discharges of cavities in ethylene propylene rubber insulation. *IEEE Trans. Dielectr. Electr. Insul.* **2014**, *21*, 1647–1659. [[CrossRef](#)]
26. Alshaikh Saleh, M.; Refaat, S.S.; Olesz, M.; Abu-Rub, H.; Guziński, J. The effect of protrusions on the initiation of partial discharges in XLPE high voltage cables. *Bull. Pol. Acad. Sci. Tech. Sci.* **2021**, *69*, e136037. [[CrossRef](#)]
27. Dissado, L.A.; Dodd, S.J.; Champion, J.V.; Williams, P.I.; Alison, J.M. Propagation of electrical tree structures in solid polymeric insulation. *IEEE Trans. Dielectr. Electr. Insul.* **1997**, *4*, 259–279. [[CrossRef](#)]
28. Chen, X.; Mantsch, A.R.; Hu, L.; Gubanski, S.M.; Blennow, J.; Olsson, C.O. Electrical treeing behavior of DC and thermally aged polyethylenes utilizing wire-plane electrode geometries. *IEEE Trans. Dielectr. Electr. Insul.* **2014**, *21*, 45–52. [[CrossRef](#)]
29. Ross, R. Inception and propagation mechanisms of water treeing. *IEEE Trans. Dielectr. Electr. Insul.* **1998**, *5*, 660–680. [[CrossRef](#)]

30. Li, J.; Zhao, X.; Yin, G.; Li, S.; Zhao, J.; Ouyang, B. The effect of accelerated water tree ageing on the properties of XLPE cable insulation. *IEEE Trans. Dielectr. Electr. Insul.* **2011**, *8*, 1562–1569. [[CrossRef](#)]
31. Fard, M.A.; Farrag, M.E.; McMeekin, S.; Reid, A. Electrical treeing in cable insulation under different HVDC operational conditions. *Energies* **2018**, *11*, 2406. [[CrossRef](#)]
32. Liu, H.; Zhang, M.; Liu, Y.; Xu, X.; Liu, A. Growth and partial discharge characteristics of DC electrical trees in cross-linked polyethylene. *IEEE Trans. Dielectr. Electr. Insul.* **2019**, *26*, 1965–1972. [[CrossRef](#)]
33. Liu, F.; Rowland, S.M.; Zheng, H.; Peesapati, V. Electrical tree growth in LDPE: Fine channel development during negative DC ramp down. *IEEE Trans. Dielectr. Electr. Insul.* **2022**, *29*, 1218–1220. [[CrossRef](#)]
34. Drissi-Habti, M.; Raj-Jiyoti, D.; Vijayaraghavan, S.; Fouad, E.-C. Numerical Simulation for Void Coalescence (Water Treeing) in XLPE Insulation of Submarine Composite Power Cables. *Energies* **2020**, *13*, 5472. [[CrossRef](#)]
35. Miceli, M.; Carvelli, V.; Drissi-Habti, M. Modelling electro-mechanical behaviour of an XLPE insulation layer for Hi-Voltage composite power cables: Effect of voids on onset of coalescence. *Energies* **2023**, *16*, 4620. [[CrossRef](#)]
36. Chen, G.; Davies, A.E. The influence of defects on the short-term breakdown characteristics and long-term dc performance of LDPE insulation. *IEEE Trans. Dielectr. Electr. Insul.* **2000**, *7*, 401–407. [[CrossRef](#)]
37. Mazzanti, G.; Montanari, G.C.; Civenni, F. Model of inception and growth of damage from microvoids in polyethylene-based materials for HVDC cables—Part 1: Theoretical approach. *IEEE Trans. Dielectr. Electr. Insul.* **2007**, *14*, 1242–1254. [[CrossRef](#)]
38. Mazzanti, G.; Montanari, G.C.; Civenni, F. Model of inception and growth of damage from microvoids in polyethylene-based materials for HVDC cables. 2. Parametric Investigation and Data Fitting. *IEEE Trans. Dielectr. Electr. Insul.* **2007**, *14*, 1255–1263. [[CrossRef](#)]
39. Niemeyer, L. A generalized approach to partial discharge modeling. *IEEE Trans. Dielectr. Electr. Insul.* **1995**, *2*, 510–528. [[CrossRef](#)]
40. Pan, C.; Chen, G.; Tang, J.; Wu, K. Numerical modeling of partial discharges in a solid dielectric-bounded cavity: A review. *IEEE Trans. Dielectr. Electr. Insul.* **2019**, *26*, 981–1000. [[CrossRef](#)]
41. Zhan, Y.; Chen, G.; Hao, M.; Pu, L.; Zhao, X.; Sun, H.; Wang, S.; Guo, A.; Liu, J. Comparison of two models on simulating electric field in HVDC cable insulation. *IEEE Trans. Dielectr. Electr. Insul.* **2019**, *26*, 1107–1115. [[CrossRef](#)]
42. Kumara, S.; Serdyuk, Y.V.; Jeroense, M. Calculation of electric fields in HVDC cables: Comparison of different models. *IEEE Trans. Dielectr. Electr. Insul.* **2012**, *28*, 1070–1078. [[CrossRef](#)]
43. Eoll, C.K. Theory of stress distribution in insulation of high-voltage DC cables: Part I. *IEEE Trans. Electr. Insul.* **1975**, *EI-10*, 27–35. [[CrossRef](#)]
44. Buller, F.H. Calculation of electrical stresses in DC cable insulation. *IEEE Trans. Power Appar. Syst.* **1967**, *PAS-86*, 1169–1178. [[CrossRef](#)]
45. Baferani, M.A.; Shahsavarian, T.; Li, C.; Tefferi, M.; Jovanovic, I.; Cao, Y. Electric field tailoring in HVDC cable joints utilizing electro-thermal simulation: Effect of field grading materials. In Proceedings of the 2020 IEEE Electrical Insulation Conference (EIC), Knoxville, TN, USA, 22 June–3 July 2020; pp. 400–404.
46. Qin, S.; Boggs, S. Design considerations for high voltage DC components. *IEEE Electr. Insul. Mag.* **2012**, *28*, 36–44. [[CrossRef](#)]
47. CIGRE Working Group D1.23. *Diagnostics and Accelerated Life Endurance Testing of Polymeric Materials for HVDC Application*; CIGRE Technical Brochure 636; CIGRE: Paris, France, 2015.
48. Hampton, R.N. Some of the considerations for materials operating under high-voltage, direct-current stresses. *IEEE Electr. Insul. Mag.* **2008**, *24*, 5–13. [[CrossRef](#)]
49. Li, Z.; Du, B. Polymeric insulation for high-voltage dc extruded cables: Challenges and development directions. *IEEE Electr. Insul. Mag.* **2018**, *34*, 30–43. [[CrossRef](#)]
50. Fu, M.; Chen, G.; Dissado, L.A.; Fothergill, J.C. Influence of thermal treatment and residues on space charge accumulation in XLPE for DC power cable application. *IEEE Trans. Dielectr. Electr. Insul.* **2007**, *14*, 53–64. [[CrossRef](#)]
51. Mazzanti, G. Issues and challenges for HVDC extruded cable systems. *Energies* **2021**, *14*, 4504. [[CrossRef](#)]
52. Reed, C.W. An assessment of material selection for high voltage DC extruded polymer cables. *IEEE Electr. Insul. Mag.* **2017**, *33*, 22–26. [[CrossRef](#)]
53. Maruyama, S.; Ishii, N.; Shimada, M.; Kojima, S.; Tanaka, H.; Asano, M.; Yamanaka, T.; Kawakami, S. Development of a 500 kV DC XLPE cable system. *Furukawa Rev.* **2004**, *25*, 47–52.
54. Murata, Y.; Sakamaki, M.; Abe, K.; Inoue, Y.; Mashio, S.; Kashiyama, S.; Matsunaga, O.; Igi, T.; Watanabe, M.; Asai, S.; et al. Development of high voltage DC XLPE cable system. *SEI Tech. Rev.* **2013**, *76*, 55–62.
55. Gu, X.; Zhu, T. Simulation of electrical field distribution of HVDC and EHVDC cable during load cycles in type test. In Proceedings of the 2022 IEEE Conference on Electrical Insulation and Dielectric Phenomena (CEIDP), Denver, CO, USA, 30 October–2 November 2022; pp. 83–86. [[CrossRef](#)]
56. Zhu, Y.; Yang, F.; Xie, X.; Cao, W.; Sheng, G.; Jiang, X. Studies on electric field distribution and partial discharges of XLPE cable at DC voltage. In Proceedings of the 2018 12th International Conference on the Properties and Applications of Dielectric Materials (ICPADM), Xi'an, China, 20–24 May 2018; pp. 562–565. [[CrossRef](#)]
57. Naderiallaf, H.; Seri, P.; Montanari, G.C. Investigating conditions for an unexpected additional source of partial discharges in DC cables: Load power variations. *IEEE Trans. Power Deliv.* **2021**, *36*, 3082–3090. [[CrossRef](#)]
58. Rizzo, G.; Romano, P.; Imburgia, A.; Ala, G. Partial discharges in HVDC cables—The effect of the temperature gradient during load transients. *IEEE Trans. Dielectr. Electr. Insul.* **2021**, *28*, 1767–1774. [[CrossRef](#)]

59. Huang, Z.Y.; Pilgrim, J.A.; Lewin, P.L.; Swingler, S.G.; Tzemis, G. Thermal-electric rating method for mass-impregnated paper-insulated HVDC cable circuits. *IEEE Trans. Power Deliv.* **2015**, *30*, 437–444. [[CrossRef](#)]
60. Diban, B.; Mazzanti, G.; Seri, P. Life-based geometric design of HVDC cables—Part I: Parametric analysis. *IEEE Trans. Dielectr. Electr. Insul.* **2022**, *29*, 973–980. [[CrossRef](#)]
61. Diban, B.; Mazzanti, G.; Seri, P. Life-based geometric design of HVDC cables—Part 2: Effect of electrical and thermal transients. *IEEE Trans. Dielectr. Electr. Insul.* **2023**, *30*, 97–105. [[CrossRef](#)]
62. Fruth, B.; Niemeyer, L. The importance of statistical characteristics of partial discharge data. *IEEE Trans. Electr. Insul.* **1992**, *27*, 60–69. [[CrossRef](#)]
63. Gutfleisch, F.; Niemeyer, L. Measurement and simulation of PD in epoxy voids. *IEEE Trans. Dielectr. Electr. Insul.* **1995**, *2*, 729–743. [[CrossRef](#)]
64. Callender, G.; Lewin, P.L. Modeling partial discharge phenomena. *IEEE Electr. Insul. Mag.* **2020**, *36*, 29–36. [[CrossRef](#)]
65. Tefferi, M. Characterization of Conduction Properties of DC Cable Dielectric Materials. Ph.D. Thesis, University of Connecticut, Storrs, CT, USA, 2019.
66. Khalil, M.S.; Gastli, A. Investigation of the dependence of DC insulation resistivity of ultra-clean polyethylene on temperature and electric field. *IEEE Trans. Power Deliv.* **1999**, *14*, 699–704. [[CrossRef](#)]
67. Weedy, B.M.; Chu, D. HVDC extruded cables—Parameters for determination of stress. *IEEE Trans. Power Appar. Syst.* **1984**, *PAS-103*, 662–667. [[CrossRef](#)]
68. Boggs, S.; Damon, D.H.; Hjerrild, J.; Holboll, J.T.; Henriksen, M. Effect of insulation properties on the field grading of solid dielectric DC cable. *IEEE Trans. Power Deliv.* **2001**, *16*, 456–461. [[CrossRef](#)]
69. Vu, T.T.N.; Teyssedre, G.; Le Roy, S. Electric field distribution in HVDC cable joint in non-stationary conditions. *Energies* **2021**, *14*, 5401. [[CrossRef](#)]
70. He, M.; Hao, M.; Chen, G.; Chen, X.; Li, W.; Zhang, C.; Wang, H.; Zhou, M.; Lei, X. Numerical modelling on partial discharge in HVDC XLPE cable. *COMPEL—Int. J. Comput. Math. Electr. Electron. Eng.* **2018**, *37*, 986–999. [[CrossRef](#)]
71. He, M.; Chen, G.; Lewin, P.L. Field distortion by a single cavity in HVDC XLPE cable under steady state. *High Volt.* **2016**, *1*, 107–114. [[CrossRef](#)]
72. He, M.; Hao, M.; Chen, G.; Li, W.; Zhang, C.; Chen, X.; Wang, H.; Zhou, M.; Lei, X. Numerical study of influential factors on partial discharges in HVDC XLPE cables. *COMPEL—Int. J. Comput. Math. Electr. Electron. Eng.* **2018**, *37*, 1110–1117. [[CrossRef](#)]
73. Mikrut, P.; Zydron, P. Partial discharge modeling in a gaseous inclusion located on the radius of a loaded HVDC XLPE cable. In Proceedings of the XVII Conference Progress in Applied Electrical Engineering (PAEE 2023), Kościelisko, Poland, 26–30 June 2023.
74. Khalil, M.S. International research and development trends and problems of HVDC cables with polymeric insulation. *IEEE Electr. Insul. Mag.* **1997**, *13*, 35–47. [[CrossRef](#)]
75. Kaminaga, K.; Ichihara, M.; Jinno, M.; Fujii, O.; Fukunaga, S.; Kobayashi, O.; Watanabe, K. Development of 500-kV XLPE cables and accessories for long-distance underground transmission lines. V. Long-term performance for 500-kV XLPE cables and joints. *IEEE Trans. Power Deliv.* **1996**, *11*, 1185–1194. [[CrossRef](#)]
76. Fromm, U.; Kreuger, F.H. Statistical behaviour of internal partial discharges at DC voltage. *Jpn. J. Appl. Phys.* **1994**, *33*, 6708–6715. [[CrossRef](#)]
77. Morshuis, P.H.F.; Smit, J.J. Partial discharges at DC voltage: Their mechanism, detection and analysis. *IEEE Trans. Dielectr. Electr. Insul.* **2005**, *12*, 328–340. [[CrossRef](#)]
78. Florkowski, M. Influence of insulating material properties on partial discharges at DC voltage. *Energies* **2020**, *13*, 4305. [[CrossRef](#)]

Disclaimer/Publisher’s Note: The statements, opinions and data contained in all publications are solely those of the individual author(s) and contributor(s) and not of MDPI and/or the editor(s). MDPI and/or the editor(s) disclaim responsibility for any injury to people or property resulting from any ideas, methods, instructions or products referred to in the content.